Delayed-neutron emission probabilities of separated isotopes of Br, Rb, I, and Cs†

P. L. Reeder, J. F. Wright,* and L. J. Alquist
Battelle, Pacific Northwest Laboratories, Richland, Washington 99352
(Received 20 September 1976)

Delayed-neutron emission probabilities (P_n) were measured for 16 isotopes of Br, Rb, I, and Cs. Sources of chemically and mass separated nuclides were obtained from an on-line mass spectrometer facility. Neutrons were counted in a multitube polyethylene-moderated detector. The total number of precursor atoms was determined by direct counting of ions deposited on the first dynode of an electron multiplier. The P_n values from this work generally agree with earlier measurements for the longer-lived precursors but are consistently higher for the shorter-lived precursors. A log-log plot of P_n versus the reduced energy window $(Q_\beta - B_n)/(Q_\beta - C)$ gives a straight line with a slope of 6.0 ± 1.4 in agreement with simplified theoretical predictions. Half-lives of Rb and Cs nuclides measured by neutron decay curves are given.

[RADIOACTIVITY ^{87,88,89}Br, ^{92,93,94,95,96,97}Rb ^{137,138}I, ^{141,142,143,144,145}Cs; measured P_n, $T_{1/2}$; on-line mass separation, polyethylene-moderated neutron counter.]

I. INTRODUCTION

Delayed neutron studies of Br, Rb, I, and Cs precursors are currently in progress at the on-line mass spectrometer facility SOLAR. The preceding paper[1] described a large polyethylene-moderated neutron counter having three rings of ^{3}He counter tubes and presented average neutron energies based on ring ratio measurements for 16 precursors. The present paper discusses delayed-neutron emission probabilities (P_n) measured by simultaneous counting of delayed neutrons and the number of precursor nuclei.

The study of delayed neutrons is of interest both for its practical applications in nuclear reactor kinetics[2,3] and for understanding the structure and decay of nuclides very far from stability.[4]

The delayed-neutron emission probability of a particular precursor is defined as the fraction of the total β decay which leads to neutron emission from excited states of the daughter (emitter) nuclide. Early attempts to measure this quantity were based on fast radiochemical separations of a particular element and resolution of the complex neutron decay curve into components representing the various isotopes of that element. The P_n value was obtained by dividing the delayed-neutron yield by the cumulative fission yield determined in other experiments or from fission yield systematics.[5,6] The advent of on-line mass spectrometers and isotope separators has led to a number of direct measurements of P_n in which the β decay and neutron decay of a single precursor were observed.[7-10] The review paper by Tomlinson contains a summary of all P_n data up to 1973.[11]

II. EXPERIMENTAL DETAILS

A. Methods

The primary method A used in this work is a direct technique based on simultaneous determination of the total number of neutrons and the total number of precursor nuclei from mass separated samples. A single mass ion beam was deposited on the first dynode of an electron multiplier detector which registered the total number of nuclei present. The electron multiplier was surrounded by a large neutron counter which recorded the total number of delayed neutrons. For this method, P_n is calculated from

$$P_n = \frac{(n \text{ counts})/\epsilon_n}{(\text{ion counts})/\epsilon_I}, \quad (1)$$

where ϵ_n and ϵ_I are the neutron counter efficiency and the ion counter efficiency, respectively. This method requires that no nuclide other than the desired precursor is present in the ion beam and that corrections be made for buildup of β activity in the electron multiplier. To account for the β activity, the ion beam was periodically switched off. Pulses from the electron multiplier were recorded in separate scalers for beam-on and beam-off time intervals. A computer calculation which took into account growth and decay of precursor and daughter nuclides was used to determine the ratio of β activities during the beam-on and beam-off time intervals. Thus the beam-off scaler count multiplied by the calculated ratio gave the β correction to the beam-on ion scaler. Repetitive cycles were accumulated until sufficient statistical accuracy was achieved. The neutron scaler was

on continuously during the experimental run.

A secondary method B of determining P_n was also employed in some of the experiments. This method was based on an equivalent definition of P_n as the ratio of saturation neutron activity $A_{sat}(n)$ to saturation β activity $A_{sat}(\beta)$. The saturation β activity is equal to the ion deposition rate for a pure beam. Experimentally the ion deposition rate was obtained from the ion counting rate R_I divided by the ion counting efficiency ϵ_I. The saturation neutron activity was obtained by resolving the precursor activity from a neutron decay curve. The initial neutron activity of the precursor $A_0(n)$ divided by the neutron counting efficiency ϵ_n and the saturation factor $1-e^{-\lambda t_b}$ (t_b is the ion deposition time) gave the saturation neutron activity for a single period of ion deposition. However, the neutron decay curves were obtained by summing the neutron activity from many successive periods of ion deposition. A multiple-pulsing correction was needed to account for neutron activity due to decay of ions deposited in previous cycles. The observed initial neutron activity $A_0^{obs}(n)$ was assumed to be the sum of an infinite series of terms

$$A_0^{obs}(n)=\sum_{i=0} A_0(n)e^{-i\lambda\tau},$$

where τ is the time between successive cycles. This expression reduces to

$$A_0^{obs}(n)=\frac{A_0(n)}{1-e^{-\lambda\tau}}.$$

The saturation neutron activity becomes

$$A_{sat}(n)=\frac{A_0^{obs}(n)(1-e^{-\lambda\tau})}{\epsilon_n(1-e^{-\lambda t_b})}.$$

Therefore P_n is given by

$$P_n=\frac{A_{sat}(n)}{A_{sat}(\beta)}=\frac{A_0^{obs}(n)}{\epsilon_n}\frac{(1-e^{-\lambda\tau})}{(1-e^{-\lambda t_b})}\frac{\epsilon_I}{R_I}. \qquad (2)$$

Methods A and B used identical detectors and so both methods have the same uncertainties in the neutron counter efficiency and ion counter efficiency. Method A has the advantage of faster data collection rates. Method B, on the other hand, has the advantage of resolving precursor neutron activity from background through analysis of a decay curve. In practice method A data was taken simultaneously when method B data was being obtained.

B. SOLAR facility

The SOLAR facility is an on-line mass spectrometer which provides chemically and mass separated beams of Br, Rb, I, and Cs nuclides.[1,12] Chemical selection is achieved by surface ionization to give positive ions of Rb^+ and Cs^+ or negative ions of Br^- and I^-. The target/ion source is similar to the Klapisch/Bernas source,[13,14] but is modified to include a separately heated chimney. By running the chimney at a lower temperature than the oven, the ratio of Rb^+ and Cs^+ to unwanted Sr^+ and Ba^+ can be greatly enhanced without losing the advantage of fast diffusion of Rb^+ and Cs^+ from the hot oven. No background peaks in the mass region of the Rb^+ and Cs^+ delayed-neutron precursors were observed.

The negative ion beams were 100 times less intense than the positive ion beams and were much less reliable. The maximum ion count rate was about 3000 ions/sec for ^{87}Br. Background peaks due to stable ions were present at masses 87–89 for which corrections to the precursor ion count rate had to be made. Typical corrections amounted to 23% at mass 87, 5% at mass 88, and 6% at mass 89. No corrections were needed for the I precursors.

C. Electron multiplier detector

The electron multipliers used in this work have 17 stages with CuBe dynodes. A pulse height spectrum of individual ions striking the first dynode is shown in Fig. 1. A discriminator was set in the deep valley between the noise pulses and the ion pulses. All pulses above the discriminator were recorded by the scalers. To determine the absolute efficiency of the ion counting system, it was necessary to estimate the number of true ion pulses smaller than the discriminator cutoff. This was done by extrapolating the low energy portion of the ion pulse height spectrum to the baseline as indicated by the dashed line in Fig. 1. The absolute ion counting efficiency was taken as the integral of the ion counts above the discriminator divided by the sum of that integral plus the area below the disciminator under the dashed line in Fig. 1. This determination was made for each of the absolute P_n measurements on ^{94}Rb and ^{143}Cs as discussed in Sec. II G.

After about 6 months in the SOLAR vacuum system, the pulse amplitude from the electron multipliers deteriorated due to aging of the dynode surfaces. Consequently the ion counting efficiency for the absolute P_n measurements ranged from (70 ±2)% to (95 ±2)% depending on the age of the electron multiplier. No short term drifts in the stability of the electron multiplier or discriminator were ever observed so it was assumed that all runs taken on the same day had equal ion counting efficiency. Pulse height spectra for stable ^{87}Rb and ^{133}Cs gave the same efficiency within the 2% uncertainty associated with the extrapolation below

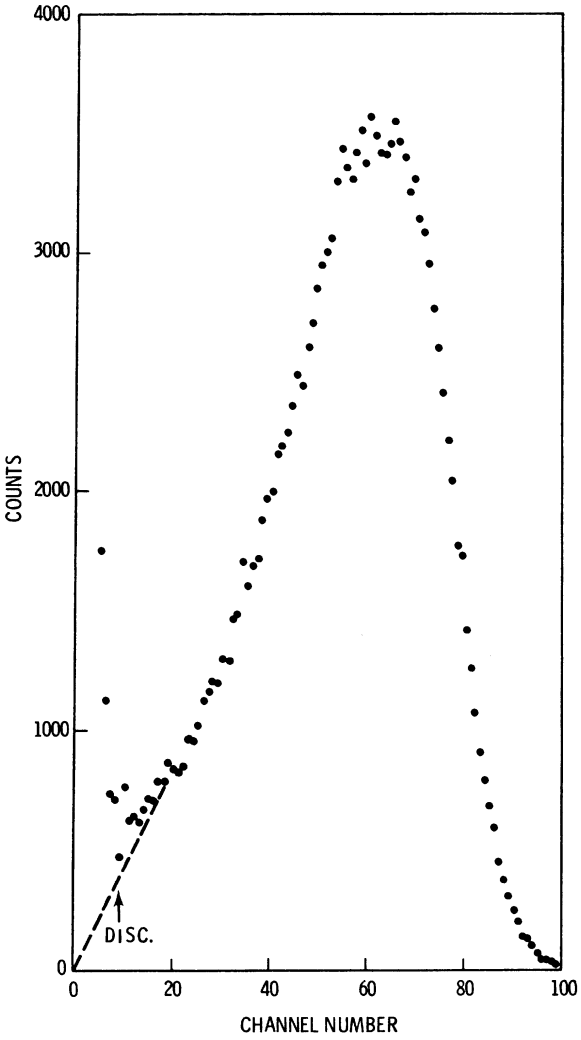

FIG. 1. Pulse height spectrum from electron multiplier detector for ^{85}Rb ion beam. 93% of the ion pulses are above the discriminator setting.

the discriminator so no mass dependent correction was made to the absolute ion efficiency. The first dynode was operated at ground potential so the same efficiency was used for both positive and negative ion beams.

D. Neutron counter

The neutron counter consisted of 42 ^{3}He counter tubes arranged in three concentric rings in a large block of polyethylene. The construction of the counter and the experimental determination of its absolute efficiency as a function of neutron energy are described in detail in the preceding paper.[1]

For all the method B runs, pulses from the middle and outer rings fed the same multiscaler. Thus the middle and outer rings were combined to give the neutron decay curves used to obtain $A_0(n)$ for method B. For method A, neutron counts from all three rings were added.

Because each precursor emits a spectrum of neutron energies, it was necessary to determine effective efficiencies for each precursor for each ring of counter tubes. As described in the preceding paper, the effective efficiency was calculated from $\epsilon^{\text{eff}}=\sum N(E)\epsilon(E)/\sum N(E)$, where $N(E)$ was the neutron spectrum for a particular precursor taken from the work of Shalev and Rudstam[4] and $\epsilon(E)$ was the efficiency curve for monoenergetic sources given in Fig. 4 of the preceding paper. These effective efficiencies were plotted versus the average energy of Shalev and Rudstam's spectra (calculated from $E_{\text{av}}=\sum N(E)E/\sum N(E)$) as shown in Fig. 2 in order to obtain calibration curves for each ring of counters. For a particular precursor the average energy as determined by ring ratios in the preceding paper was used to determine the effective efficiency from the calibration curve even though this average energy may have differed from that calculated from Shalev and Rudstam's spectrum. It should be noted that the use of Shalev and Rudstam's spectra to determine the correction to the calibration curve based on monoenergetic sources may not be exact since their spectra do not extend below about 100 keV and since other workers[15] have obtained somewhat "harder" spectra for two of the same precursors. However, the effective efficiencies are not very sensitive to the detailed shape of the neutron spectrum. This can be seen in Fig. 2 by comparing the efficiencies for monoenergetic sources (shown as points with error bars) with the smooth curves drawn through the effective efficiencies (points without error bars).

E. Electronics

A schematic diagram of the electronics for the P_n measurements is shown in Fig. 3. The digital timing unit[16] provided automatic control of the ion beam and scalers. The neutron scalers were gated on when the timing unit was started and they stayed on until the timing unit was stopped. A scaler not shown recorded the elapsed time from start to finish. The timing unit also provided adjustable time intervals for beam on and beam off during each cycle. The number of cycles was recorded in another scaler also not shown.

The ion beam was switched off at the ion source by adding 80 V to the voltage applied to one of the beam centering plates in the ion lens. Measurement of the switching time showed that it took 0.2 μ sec for the ion beam to be completely switched off. This delay meant a few unwanted ion pulses

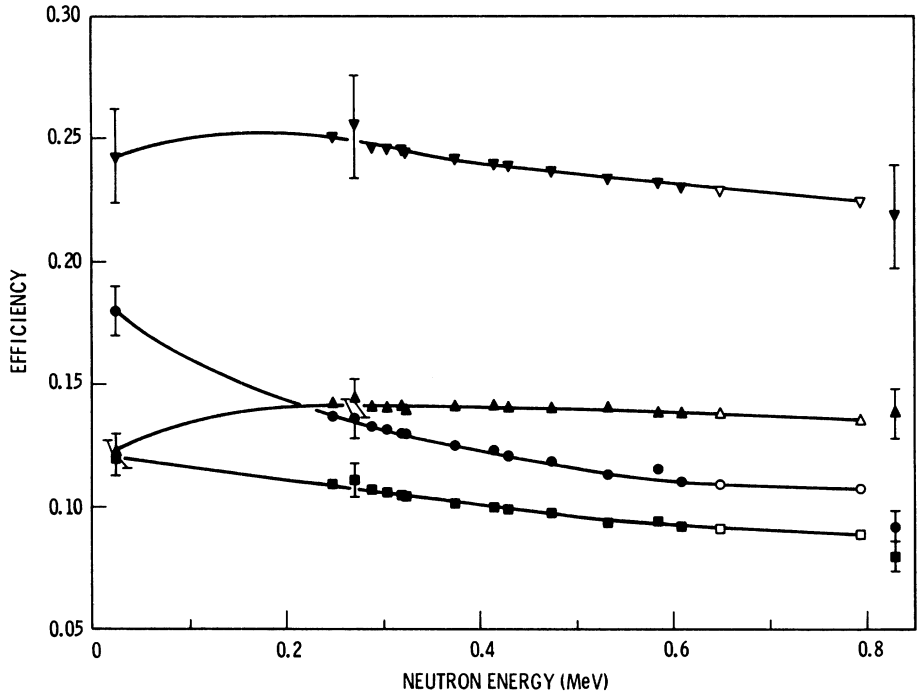

FIG. 2. Calibration curves of neutron counter efficiency versus neutron energy: ●, inner ring; ■, middle ring; ▲, outer ring; ▼, outer plus middle. Points with error bars are for monoenergetic (γ, n) sources. Closed points without error bars are effective efficiencies versus average energy based on the Shalev-Rudstam spectra (Ref. 4). Open points are based on Franz *et al.* spectra (Ref. 15).

were counted by the beam off scaler. However, the shortest time interval used for the beam off scaler was 200 msec and calculations showed that the counts due to the switching time delay were negligible in all cases.

In Fig. 3 the dashed lines indicate the two 400-channel multiscalers used in method B for storing decay curves. The start of the multiscaling could be synchronized by the timing unit either to the beam-on time or the beam-off time, but in any case the multiscalers covered both beam on and beam off. The neutron multiscaler curve showed growth during the beam-on interval and decay during the beam-off interval, but only the decay curve was analyzed to obtain $A_0(n)$. The multiscaler curve from the electron multiplier was analyzed both during beam on and beam off in order to obtain the average ion deposition rate as discussed below.

The ion beam stability was monitored pulse by pulse by a count rate meter driven by pulses from the electron multiplier. Changes in the ion deposition rate were due primarily to long term drifts of the magnetic field in the mass analyzing magnet. Slight adjustments to the magnetic field were made as needed to maintain constant ion deposition rates.

F. Data collection

The time intervals used for beam on and beam off were adjusted to be some multiple of the precursor half-life. The multiples commonly used are shown in Table I.

Because long-lived daughter activities led to a gradual buildup of background on the electron multiplier, experimental runs were begun on the lowest yield (highest mass number) isotope of the particular element being studied. Background counting rates on both the electron multiplier and neutron counter were measured by 100 sec runs taken both before and after the data runs. As mentioned in the preceding paper, backgrounds in the neutron counter were constant as long as the temperature of the oven was constant. All neutron backgrounds taken at the same temperature were

TABLE I. Time intervals in multiples of the precursor half-life.

Method	Time on	Time off
A	1	1
A	1	3
A, B	2	8

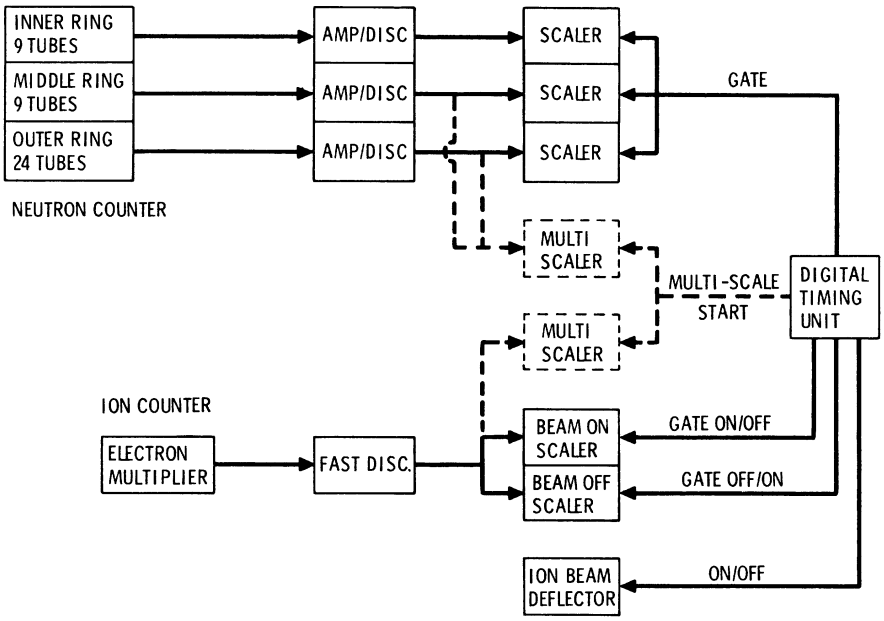

FIG. 3. Schematic diagram of counting electronics for P_n measurements.

combined to give better statistical accuracy. The background of the electron multiplier depended greatly on the nature and quantity of the ions previously deposited. The time interval between data runs was usually long enough to insure that long-lived daughter activities from a previous run had reached a steady state before starting the new data run. Normally only the background counting rate taken just before the start of the new data run was used to determine the electron multiplier background. In a few cases a variable background was used based on the known decay rates of the daughters of the previous run.

G. Data analysis and corrections

The experimental data obtained for method A consisted of the electron multiplier scaler counts during beam on (A_1) and during beam off (A_2), the total neutron counts over the entire run A_3, and respective background counts for both the neutron and electron multiplier detectors (B_1, B_2, and B_3). Because the electron multiplier was sensitive to β particles from decay of the radioactive nuclides deposited on the first dynode, the data recorded in the electron multiplier beam-on scaler included a contribution equal to $\epsilon_\beta N_\beta^{on}$ and the data recorded in the beam-off scaler included a contribution equal to $\epsilon_\beta N_\beta^{off}$ where ϵ_β is the β counting efficiency of the electron multiplier, N_β^{on} represents the total number of β decays of the precursor and its daughters during the beam on interval, and N_β^{off} is the same quantity for the beam-off interval. The total number of neutrons from the precursor is given by $(A_3 - B_3)/\epsilon_n$. The total number of precursor ions deposited is given by $[(A_1 - B_1) - (A_2 - B_2)(N_\beta^{on}/N_\beta^{off})]/\epsilon_I$. Equation (1) for P_n then becomes

$$P_n = \frac{(A_3 - B_3)/\epsilon_n}{[(A_1 - B_1) - (A_2 - B_2)(N_\beta^{on}/N_\beta^{off})]/\epsilon_I} . \qquad (3)$$

Equation (3) includes the assumption that the β counting efficiency is the same for both time intervals. This is true if the precursor and its daughters all have the same counting efficiency or if each nuclide contributes the same fraction of the total β activity in both time intervals. When both time intervals were set equal to one half-life of the precursor, calculations showed that the precursor contributed the same fraction of the total activity in both time intervals. Values of P_n determined under these conditions were identical to values determined under conditions where daughter activities were enhanced in the beam-off interval. Thus the assumption of equal β counting efficiencies in Eq. (3) is valid.

The calculation of the β activities is complicated by the necessity of including the growth and decay of daughter and granddaughter activities for both the direct β branch and the delayed-neutron branch. The half-lives of these four nuclides are long compared to the cycle time of the pulsed beam experiments so it is necessary to make corrections for buildup from cycle to cycle (multiple-pulsing correction). The delayed-neutron emission probability is one of the parameters appear-

ing in the calculation of N_β^{on} and N_β^{off}. Equation (3) then becomes a quadratic expression for P_n with one physical solution and one nonphysical solution. We have derived exact expressions for calculating the β activities in combination with the quadratic expression for P_n and have solved these expressions for P_n.[17]

The absolute value of P_n depends critically on the neutron counter efficiency and the ion counting efficiency. To eliminate the effect of possible variations of counter efficiencies from day to day, the P_n values on a particular day were calculated relative to the P_n's for ^{94}Rb or ^{143}Cs which in the SOLAR facility are the isotopes with the highest neutron counting rates for their respective elements. The relative values for a particular precursor from runs taken on different days were combined into the weighted averages shown in Table II. Relative P_n values for the halogens were calculated with respect to ^{143}Cs which was measured on the same or neighboring days. All the relative P_n values include the use of the energy dependent neutron counter efficiencies which were discussed in Sec. II D and which are listed for each precursor in Table II. The absolute P_n's are based on four measurements on ^{94}Rb and five measurements on ^{143}Cs for which the ion counting efficiencies were accurately measured.

For method B, the delayed-neutron decay curves were analyzed by a least squares computer code CLSQ[18] into two components—one with the half-life of the delayed-neutron precursor and one with an infinite half-life for the background. (See Appendix.) The initial neutron activity at the time the ion beam was shut off was used for $A_0(n)$ in Eq. (2). To obtain the ion counting rate R_I both the beam-on and beam-off portions of the electron multiplier multiscaling curves were analyzed by CLSQ to obtain counting rates at the end of beam-on time (or the end of beam-off time). The net count rate at this time not due to β activity or multiplier background was due to the ion deposition rate. Absolute values of P_n for each precursor were then calculated from Eq. (2) using measured values of the ion counter efficiency and the effective efficiencies of the neutron counter outer and middle rings shown in Fig. 2.

The polyethylene in the neutron counter contained about 0.66 g of deuterium. It is conceivable that photoneutrons from high energy γ rays in the decay of the precursors or their daughters could contribute to the observed neutron counts. To check this point, a glass cylinder containing D_2O was designed to replace one of the ^{3}He neutron counters in the inner ring. The cylinder contained 18.3 g of D as 86% enriched D_2O which gave a factor of 28 times more D than in the normal counter. Method A P_n measurements were made with and without the D_2O for $^{94-97}$Rb and $^{143-145}$Cs. No change in P_n was observed which indicated that the (γ, n) effect was insignificant.

For both method A and method B measurements, it was essential that all of the ion beam strike the active area of the electron multiplier detector. If the beam spot were bigger than the first dynode, then precursor ions would be deposited inside the neutron counter and would contribute to the neutron count without giving a corresponding count on the electron multiplier. The effect on P_n would be to give unusually high P_n values.

TABLE II. Relative P_n values (method A) and effective neutron counting efficiencies.

Precursor	Number of measurements	Relative P_n	Neutron counter efficiency
^{92}Rb	2	0.00090 ± 0.00016	0.397 ± 0.044
^{93}Rb	9	0.137 ± 0.008	0.344 ± 0.043
^{94}Rb	13	1.000	0.344 ± 0.043
^{95}Rb	9	0.855 ± 0.045	0.347 ± 0.047
^{96}Rb	12	1.28 ± 0.06	0.344 ± 0.046
^{97}Rb	5	2.93 ± 0.21	0.334 ± 0.045
^{141}Cs	3	0.0217 ± 0.0034	0.387 ± 0.046
^{142}Cs	7	0.0441 ± 0.0046	0.387 ± 0.046
^{143}Cs	13	1.000	0.370 ± 0.042
^{144}Cs	10	1.91 ± 0.29	0.378 ± 0.042
^{145}Cs	10	9.4 ± 1.3	0.356 ± 0.046
^{87}Br	3	1.09 ± 0.16	0.401 ± 0.044
^{88}Br	3	3.25 ± 0.45	0.377 ± 0.045
^{89}Br	2	8.2 ± 1.1	0.334 ± 0.051
^{137}I	2	4.18 ± 0.61	0.347 ± 0.047
^{138}I	2	3.0 ± 1.8	0.347 ± 0.047

TABLE III. Delayed-neutron emission probabilities (%) from SOLAR experiments (numbers in parentheses are the number of determinations).

Nuclide	Method A	Method B	Wt. ave.[a]
^{87}Br	2.17 ±0.33 (3)	3.00 ±0.44 (3)	2.5 ±0.3
^{88}Br	6.46 ±0.95 (3)	7.79 ±0.57 (3)	7.4 ±0.5
^{89}Br	16.3 ±2.5 (2)	17.3 ±2.2 (2)	16.9 ±1.7
^{92}Rb	0.012±0.002 (2)		0.012±0.002
^{93}Rb	1.80 ±0.14 (9)	1.97 ±0.18 (1)	1.86 ±0.13
^{94}Rb	13.1 ±0.7 (4)	14.4 ±0.7 (1)	13.7 ±1.0
^{95}Rb	11.2 ±0.8 (9)	10.8 ±0.8 (2)	11.0 ±0.8
^{96}Rb	16.8 ±1.2 (12)	17.2 ±1.3 (2)	17.0 ±1.2
^{97}Rb	38.3 ±3.3 (5)	31.6 ±4.4 (1)	35.9 ±2.6
^{137}I	8.3 ±1.3 (2)	8.7 ±1.2 (2)	8.5 ±0.9
^{138}I	6.0 ±3.5 (2)	19.8 ±5.6[b] (1)	6.0 ±3.5
^{141}Cs	0.043±0.007 (3)		0.043±0.007
^{142}Cs	0.088±0.010 (7)	0.109±0.013 (1)	0.096±0.008
^{143}Cs	1.98 ±0.10 (5)	1.90 ±0.12 (2)	1.95 ±0.14
^{144}Cs	3.79 ±0.61 (10)	4.52 ±0.33 (2)	4.3 ±0.3
^{145}Cs	18.7 ±2.8 (10)	22.9 ±1.7 (2)	21.8 ±1.5

[a]The uncertainty of the weighted average is the larger of the statistical error $(\sum 1/s^2)^{-1/2}$ or the systematic error of 7% in the neutron counter calibration.
[b]Omitted from weighted average.

At the time of these experiments it was not possible to determine the actual size of the beam spot at the first dynode. The ion beam transport system was designed to give unit magnification of a slit located at the focus of the analyzing magnet. This slit was normally 1.27 cm high by 0.13 cm wide. The electron multiplier detector had a collimator 1.7 cm high by 0.6 cm wide covering the first dynode. Thus all the ion beam should have reached the first dynode provided residual gas scattering in the extended beam pipe did not expand the beam. To check this possibility the Rb and Cs P_n's were measured using a smaller slit 0.48 cm high by 0.13 cm wide. The measured P_n's were the same within the experimental uncertainties as those measured with the normal slit which indicated that the ion beam spot size was not a problem.

After the P_n experiments had been completed, the electron multiplier detector on the extended beam pipe was replaced by a chevron electron multiplier array (CEMA) and phosphor screen assembly. This detector provided a visual display of the ion beam and confirmed that the ion beam was an unmagnified image of the upstream slit.

III. RESULTS AND DISCUSSION

The delayed-neutron emission probabilities measured by method A and method B are given in Table III.

The uncertainties shown with the SOLAR data are

TABLE IV. Delayed-neutron emission probabilities (%) of Br nuclides.

Experiment \ Mass	87	88	89	90	91	92
SOLAR	2.5 ±0.3	7.4 ±0.5	16.9±1.7			
Kratz and Herrmann[a]	2.56±0.38	6.5 ±0.7	12.5±2.0	18.9±3.9	14.1±3.6	24.5±10
Izak-Biran and Amiel[b]	2.35±0.40	5.50±0.95	13.6±4.3	24.6±7.4	12.3±6.5	
Tomlinson[c]	3.1 ±0.6 2.1±0.3 2.3±0.4	6.0 ±1.6 4.3 ±0.5	7 ±2 7.2±1.8	11 ±3		

[a]Reference 6, revised values.
[b]Reference 5.
[c]Reference 11.

TABLE V. Delayed-neutron emission probabilities (%) of Rb nuclides.

Experiment \ Mass	92	93	94	95	96	97	98
SOLAR	0.012 ±0.002	1.86 ±0.13	13.7 ±1.0	11.0 ±0.8	17.0±1.2	35.9±2.6	
Roeckl *et al.*[a]		1.24 ±0.14	8.46±0.92	8.54±0.91	13.0±1.4	27.2±3.0	13.3±2.1
Asghar *et al.*[b]	0.0125±0.0015	1.164±0.081 1.2 ±0.1 1.55 ±0.65	9.6 ±0.8	8.4 ±0.5			
Izak-Biran and Amiel[c]		1.73 ±0.50	9.3 ±1.8				
Gunther *et al.*[d]					12 ±3	31 ±8	
Tomlinson[e]	0.012 ±0.004	2.6 ±0.4 1.43 ±0.18 1.59 ±0.29 2.1 ±0.6	11.1 ±1.1 11.0 ±2.0	7.10±0.93	12.7±1.5	>20	
Kratz[f]			9.68±0.5	8.38±0.5	12.5±0.9	25.2±1.8	

[a]Reference 8.
[b]References 9 and 10.
[c]Reference 5.
[d]Reference 20.
[e]Reference 11.
[f]K. L. Kratz (private communication).

dominated by the approximately 7% uncertainty in the neutron counter efficiencies. The statistical uncertainties in the counting data were usually less than 2%. The numbers in parentheses with the SOLAR data refer to the number of determinations. For method A the number of absolute determinations for ^{94}Rb and ^{143}Cs are given, whereas for the other nuclides the numbers of relative measurements are given. All method B determinations are absolute.

The SOLAR method A and method B results agree with each other within the uncertainties listed except for ^{87}Br and ^{138}I. For ^{138}I only one method B experiment was performed with relatively low count rate. The result is probably in error because it differs so greatly from all previous measurements. For ^{87}Br the disagreement between the method A and method B results is only slightly greater than the combined uncertainties. The reliability of these numbers may be affected by the rather large correction (typically 23%) for a stable impurity in the mass 87 ion beam.

In Table III, the weighted averages of the method A and method B results are given. These weighted averages are compared in Tables IV–VII with all other literature values. All measurements prior to Tomlinson's review of 1973 (Ref. 11) are listed together, whereas recent measurements are listed separately. Tomlinson's review includes P_n measurements by both the "direct" and the "radiochemical" methods. The data of Roeckl *et al.*[8] and Asghar *et al.*[9,10] are based on "direct" experiments.

In comparing the present results with the litera-

TABLE VI. Delayed-neutron emission probabilities (%) of I nuclides.

Experiment \ Mass	137	138	139	140	141
SOLAR	8.5 ±0.9	6.0 ±3.5			
Kratz and Herrmann[a]	6.06±0.51	4.5 ±0.9	10.1±3.6	21.7±5.6	39±13
Izak-Biran and Amiel[b]	6.65±1.17	5.14±2.32	13.9±6.0	50 ±30	
Tomlinson[c]	3.0 ±0.5 4.7 ±1.0 8.6 ±1.2 5.2 ±0.7	2.0 ±0.5 3.0 ±0.8	10 ±3	32 ±13	

[a]Reference 6, revised values.
[b]Reference 5.
[c]Reference 11.

TABLE VII. Delayed-neutron emission probabilities (%) of Cs nuclides.

Experiment \ Mass	141	142	143	144	145	146
SOLAR	0.043±0.007	0.096±0.008	1.95±0.14	4.3 ±0.3	21.8±1.5	
Roeckl *et al.*[a]					12.1±1.4	14.2±1.7
Asghar *et al.*[b]	0.053±0.003	0.285±0.026				
Tomlinson[c]	0.073±0.011	0.21 ±0.06	1.13±0.25	1.10±0.25		
Kratz[d]			1.74±0.12	2.95±0.25	12.2±0.9	

[a]Reference 8.
[b]References 9 and 10.
[c]Reference 11.
[d]K. L. Kratz (private communication).

ture values, the most striking feature is the more rapid increase of P_n with increasing mass number for precursors of the same element shown by the present data. This trend is in agreement with a theoretical treatment of delayed-neutron emission probabilities given by Kratz and Herrmann[19] and by Roeckl *et al.*[8] These authors show that P_n should be given by the expression

$$P_n = \left(\frac{Q_\beta - B_n}{Q_\beta - C}\right)^6 \qquad (4)$$

if one makes the simplifying assumptions that the β strength function is constant above a certain cutoff energy C, the Fermi function for β decay is approximately $(Q_\beta - E)^5$, and the competition between neutron emission and γ emission is neglected. With these simplifications P_n depends only on the β decay energy of the precursor Q_β, the neutron binding energy of the emitter B_n, and the cutoff parameter C. A log-log plot of Eq. (4) should give a straight line with a slope of 6. Previous authors have taken the available data and obtained slopes of less than 6.[6,8,19] This was explained in terms of nonconstant β strength functions. We have taken the $(Q_\beta - B_n)/Q_\beta - C)$ values for an average of four different mass formulas as given by Kratz and Herrmann[19] and have plotted the SOLAR method A data on a log-log plot shown in Fig. 4. A least squares fit of a straight line to these data gives a slope of 6.0 ±1.4 in agreement with Eq. (4).

Perhaps the discrepancy between the present results and earlier measurements may be partly due to our use of an energy dependent neutron counter efficiency. As discussed in Sec. IID and in the preceding paper, the energy dependence of the present counter was thoroughly investigated with photoneutron sources and corrections to the efficiencies have been made to account for the delayed-neutron spectra. We suggest that the previous data should be examined to see if the energy dependence of the neutron counter has been prop-

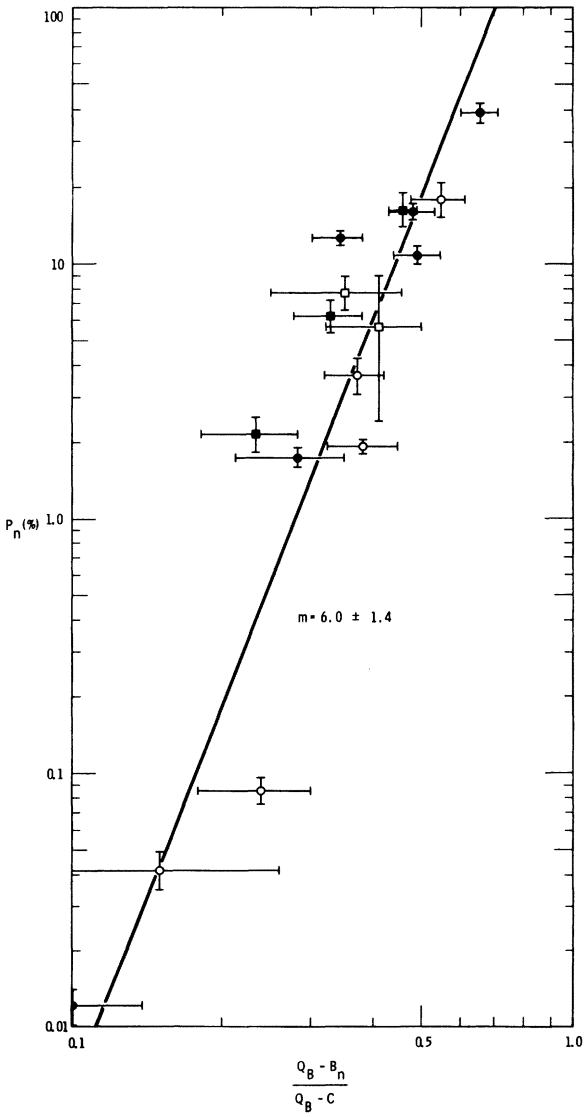

FIG. 4. Delayed-neutron emission probability versus reduced neutron energy window: ■, Br; ●, Rb; □, I; and ○, Cs.

TABLE VIII. Half-lives (sec) of neutron-rich Rb and Cs nuclides.

Mass	SOLAR (β)	SOLAR (n)	Lund and Rudstam [a]	Roeckl *et al.* [b]	Kratz [c]
92	4.54 ±0.02		4.34 ±0.06		
93	6.12 ±0.08	5.82 ±0.03	5.85 ±0.03	6.39 ±0.35	
94	2.83 ±0.03	2.73 ±0.01	2.69 ±0.02	2.76 ±0.08	2.73 ±0.02
95	0.377±0.004	0.369±0.005	0.400±0.004	0.383±0.006	0.377±0.006
96	0.205±0.004	0.197±0.002	0.203±0.003	0.199±0.004	0.197±0.005
97	0.182±0.007	0.167±0.002	0.172±0.003	0.172±0.005	0.171±0.004
142	1.70 ±0.02	1.70 ±0.09	1.69 ±0.09		
143	1.79 ±0.02	1.79 ±0.04	1.78 ±0.01		1.765±0.030
144	1.00 ±0.04	0.99 ±0.02	1.00 ±0.02		1.00 ±0.01
145	0.65 ±0.03	0.577±0.006	0.58 ±0.01	0.61 ±0.02	0.616±0.020
146		0.28 ±0.03	0.343±0.007	0.35 ±0.04	

[a] References 21 and 22.
[b] Reference 8.
[c] K. L. Kratz (private communication).

erly accounted for. For example, the present value for the P_n of ^{92}Rb is 0.012 ±0.002 in excellent agreement with the value given by Asghar *et al.* of 0.0125 ±0.0015. However, for ^{95}Rb the present value is 30% greater than that given by Asghar *et al.* The difference in neutron counter efficiency for these two precursors shown in Table II is only 14%. Even if a constant efficiency versus neutron energy curve were assumed, the present data would still give higher P_n values for nuclides farther from stability than the previous measurements. Thus there may be other systematic differences in techniques which account for the discrepancies. It should be noted that the present work involved the measurement of a large number of precursors by use of the same techniques and calibrations.

IV. SUMMARY AND CONCLUSIONS

We have presented experimental measurements of the delayed-neutron emission probabilities for 16 precursors among the Br, Rb, I, and Cs nuclides. The experimental method involved on-line mass separation and direct counting of one precursor at a time. Although the same neutron detector and ion detector were used, data collection and analysis were done by two separate methods which gave essentially identical results for the P_n values. Method A was used more frequently so the results by this method are more extensive and complete.

The P_n values measured here generally agree with earlier measurements for the longer-lived precursors. However, the P_n values for the short-lived precursors are consistently higher than earlier measurements. The present results give better agreement with the theoretical slope of a plot of $\log P_n$ versus $\log(Q_\beta - B_n)/(Q_\beta - C)$.

We wish to acknowledge N. E. Ballou for many helpful discussions and his continued support throughout this work.

APPENDIX: Rb and Cs half-lives

In connection with the CLSQ analysis of the neutron multiscaling curves for method B, the precursor half-life was varied to obtain the best fit to the decay curves.

The resulting half-lives for Rb and Cs nuclides are presented in Table VIII and are compared with other recent half-life measurements done by delayed-neutron counting.[8,21,22] Table VIII also includes our earlier measurements of these half-lives done by β counting on the electron multiplier detector.[23] The β decay curves are more complex and thus are more difficult to analyze. Thus the half-lives done by neutron counting are the preferred values in most cases.

†Work performed under ERDA, Contract No. EY-76-C-06-1830.
*Present address: Los Alamos Scientific Laboratory, University of California, Los Alamos, New Mexico 87544

[1] P. L. Reeder, J. F. Wright, and L. J. Alquist, preceding paper, Phys. Rev. C 15, 2098 (1977).
[2] G. R. Keepin, in *Delayed Fission Neutrons* (International Atomic Energy Agency, Vienna, 1968), p. 3.
[3] S. Yiftah and D. Saphier, in *Delayed Fission Neutrons* (International Atomic Energy Agency, Vienna, 1968), p. 23.

[4]S. Shalev and G. Rudstam, Nucl. Phys. A230, 153 (1974); A235, 397 (1974).
[5]T. Izak-Biran and S. Amiel, Nucl. Sci. Eng. 57, 117 (1975).
[6]K. L. Kratz and G. Herrmann, Nucl. Phys. A229, 179 (1974); (private communication).
[7]I. Amarel, H. Gauvin, and A. Johnson, J. Inorg. Nucl. Chem. 31, 577 (1969).
[8]E. Roeckl, P. F. Dittner, R. Klapisch, C. Thibault, C. Rigaud, and R. Prieels, Nucl. Phys. A222, 621 (1974).
[9]M. Asghar, J. Crancon, J. P. Gautheron, and C. Ristori, J. Inorg. Nucl. Chem. 37, 1563 (1975).
[10]M. Asghar, J. P. Gautheron, G. Bailleul, J. P. Bocquet, J. Greif, H. Schrader, G. Siegert, C. Ristori, J. Crancon, and G. I. Crawford, Nucl. Phys. A247, 359 (1975).
[11]L. Tomlinson, At. Data Nucl. Data Tables 12, 179 (1973).
[12]J. J. Stoffels, Nucl. Instrum. Methods 119, 251 (1974).
[13]R. Klapisch, J. Chaumont, C. Philippe, I. Amarel, R. Fergeau, M. Salome, and R. Bernas, Nucl. Instrum. Methods 53, 216 (1967).
[14]I. Amarel, R. Bernas, J. Chaumont, R. Foucher, J. Jastrzebski, A. Johnson, R. Klapisch, and J. Teillac, Ark, Fys. 36, 77 (1967).
[15]H. Franz, J. V. Kratz, K. L. Kratz, W. Rudolph, G. Herrmann, F. M. Nuh, S. G. Prussin, and A. A. Shihab-Eldin, Phys. Rev. Lett. 33, 859 (1974).
[16]The timing unit was part of the electronic control for a moving tape collector system kindly loaned to us by W. Talbert of Iowa State University.
[17]L. J. Alquist, J. F. Wright, and P. L. Reeder, Battelle, Pacific Northwest Laboratories, Report No. BNWL-SA-5900, SUP, 1976 (unpublished).
[18]J. B. Cumming, in *Applications of Computers to Nuclear and Radiochemistry*, edited by G. D. O'Kelley (Office of Technical Service, Washington, D.C., 1963), NAS-NS 3107 (program modified by B. Erdal).
[19]K. L. Kratz and G. Herrmann, Z. Phys. 263, 435 (1973).
[20]H. Gunther, G. Siegert, K. Wünsch, and H. Wollnik, Nucl. Phys. A242, 56 (1975).
[21]G. Rudstam and E. Lund, Phys. Rev. C 13, 321 (1976).
[22]E. Lund and G. Rudstam, Phys. Rev. C 13, 1544 (1976).
[23]P. L. Reeder and J. F. Wright, Phys. Rev. C 12, 718 (1975).